arXiv:cond-mat/0607525v1 [cond-mat.mes-hall] 20 Jul 2006

Ballistic electron spectroscopy

F. Hohls, M. Pepper, J. P. Griffiths, G. A. C. Jones, and D. A. Ritchie
Cavendish Laboratory, University of Cambridge, J J Thomson Avenue, Cambridge CB3 0HE, UK

(Dated: February 6, 2008)

We demonstrate the feasibility of ballistic electron spectroscopy as a new tool for mesoscopic physics. A quantum dot is utilised as an energy-selective detector of non-equilibrium ballistic electrons injected into a two-dimensional electron system. In this paper we use a second quantum dot as the electron injector to evaluate the scheme. We propose an application in the study of interacting 1D and 0D systems.

PACS numbers: 73.23.Ad, 73.23.Hk

Quantum dots and wires are coming to an age of application and are used as building blocks of devices with increasing complexity.[1,2] This sets high standards in the characterization and understanding of the individual elements. Non-equilibrium transport measurement, also named transport spectroscopy, is amongst the most commonly used tool to reveal characteristics of quantum wires[3] and quantum dots.[4] For one-dimensional systems, the sub-band spacing can be determined; for quantum dots, level spacing and tunnelling rates can be extracted. However, if there is strong interaction between electrons in these systems, the internal structure cannot be assumed to be independent of the applied bias voltage.

We propose instead to directly measure the energy distribution of non-equilibrium ballistic electrons leaving the device under study, allowing us to draw conclusions concerning the internal energetic structure without altering it with our measurement technique. Injection and detection of non-equilibrium electrons has been demonstrated for MBE grown and Schottky gate induced tunnelling barriers[5,6,7] and also using quantum point contacts.[8,9,10] However, these techniques do not offer true energy selectivity as electrons at all energies beyond a threshold can pass the detector. *Here* we use the controllable energy selectivity of resonant transport through a quantum dot as a spectrometer of non-equilibrium ballistic electrons which allows us to assess the complete energy distribution.

In this work we test the feasibility of our ballistic electron spectroscopy scheme using a second quantum dot for a well-defined injection of non-equilibrium electrons. The schematic of our device is shown in Fig. 1. Resonant tunnelling through the left quantum dot injects ballistic electrons into the middle two-dimensional electron system (2DES) region. Those electrons that travel ballistically to the detector dot and whose excess energy δE matches the resonance condition ($\delta E = \Delta E$) can tunnel to its drain and are detected as a current. We change the resonant energy of the detector ΔE to scan the complete spectrum of the incident ballistic electrons. A magnetic field B perpendicular to the plane of the 2DES allows us to differentiate the ballistic portion of the signal.

We use standard Schottky metal gates[11] to define our device in a high mobility 2DES in a GaAs/AlGaAs heterostrucure. The 2DES lies 90 nm beneath the surface and has a density $n_e = 1.7 \times 10^{15}$ m^{-2} and a mobility $\mu_e = 170$ m^2/Vs. The transport mean free path, l_e, is of order $12\,\mu$m, exceeding the dimensions of the device. All experiments were performed with an electronic temperature $T \lesssim 0.2$ K. For this temperature and for the excess energies of our ballistic electrons, $\delta E \leq 0.3$ meV, we expect the dominant relaxation process to be electron-electron scattering, with a scattering length $l_{e-e} \geq 10\,\mu$m.[8,12]

The gate layout is displayed as inset in Fig. 2. Two quantum dots of lithographic size 300 nm are separated by about $3\,\mu$m. The symmetry axis of the quantum dots are set at an angle to each other to avoid direct backscattering. Ohmic contacts allow independent control of the chemical potentials of all regions. With the exception of Fig. 2b we use the left quantum dot (QD1) to inject non-equilibrium ballistic electrons into the middle region. We bias the source with the sum of a negative DC-bias $V_{\rm sd}$ and a square-wave AC excitation ($\pm 50\,\mu$V). The injector level of the dot is set to resonance with the mean chemical potential of the source lead as depicted in Fig. 1. Thus we inject ballistic electrons with an excess energy of $\delta E \approx -eV_{\rm sd}$ into the middle region. The AC excitation modulates the flux of the ballistic electrons (modulation depth $\sim 50\%$) and thereby allows for a more sensitive lock-in detection scheme. Throughout the paper we only state the AC currents in response to this modulation.

The ballistic electron spectrometer is formed by the

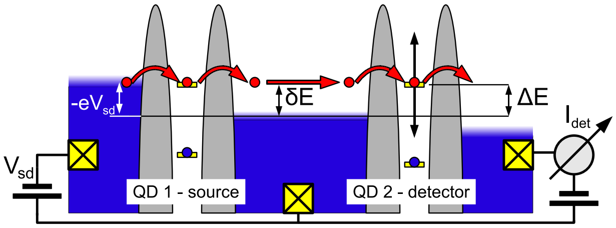

FIG. 1: Schematic of ballistic electron spectroscopy: The left quantum dot (QD1) injects non-equilibrium ballistic electrons into the middle 2DES region. Those electrons that travel to the detector quantum dot (QD2) can only tunnel to the right lead if their energy matches one of the detector dot states, the energy of which can be tuned by a gate. Recording the current I as function of the dot energy allows measurement of the spectrum of the incident electrons.

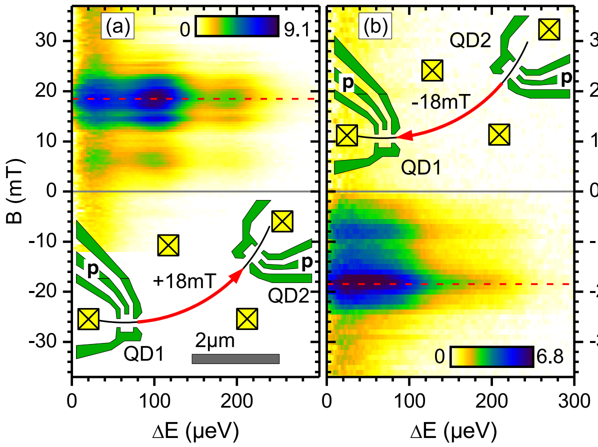

FIG. 2: Current I_{det} [pA] measured by the detector dot as a function of detector energy ΔE and magnetic field B for $200\,\mu$eV injector energy. Panel (a) shows injection by QD1 (injected current $I_{\mathrm{inj}} \approx 280\,$pA) and detection by QD2, panel (b) shows the result of swapping injection and detection quantum dots ($I_{\mathrm{inj}} \approx 210\,$pA). The dashed lines at $B = \pm 18.5\,$mT mark the positions of maximum signal which reverses in B for the two configurations. *Insets:* Layout of the device; 'p' marks the plunger gate used to tune the dot energy. The crossed squares indicate ohmic contacts. Injected ballistic electrons travel along a curved path, $r_c = 65\,\mu\mathrm{m}/B\,[\mathrm{mT}]$. The paths shown have radius $3.6\,\mu$m corresponding to $\pm 18\,$mT.

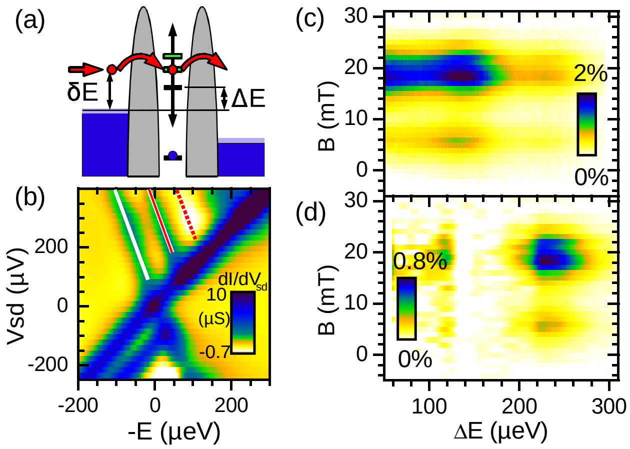

FIG. 3: a) Schematic of detected signal due to tunnelling via excited states causing replica signal at apparent lower energies. b) Bias characterization of the detector dot reveals excited states. The white line marks the ground state resonance with the source, the red lines mark the resonances due to the excited states discussed in the text. c) Normalized detector signal $I_{\mathrm{det}}/I_{\mathrm{inj}}$ as measured (injection by QD1 set to $\approx 230\,\mu$eV, detection by QD2). d) Deconvolved signal when considering two excited states.

detector quantum dot (QD2 except for Fig. 2b): its resonant transmission energy ΔE is tuned by a plunger gate and the transmitted current is measured by a lock-in technique at the injector modulation frequency. A small bias voltage ($+100\,\mu$V) across the detector (see Fig. 1) improves the ballistic electron signal at small energies ΔE. The $\Delta E = 0$ point is determined for each spectrometer sweep using the current response to a small AC voltage ($5\,\mu$V) applied across the detector dot. The conversion factors from plunger gate voltage V_{p} to energy ΔE were determined from bias spectroscopy measurements of the individual dots.

We apply a small perpendicular magnetic field which forces the ballistic electrons into a cyclotron orbit with radius $r_c = 65\,\mu\mathrm{m}/B\,[\mathrm{mT}]$. The device design ensures that the injected ballistic electrons can reach the detector only for a non-zero magnetic field that gives the right curvature of the ballistic path. This allows direct ballistic electrons to be distinguished from scattered ones.

Fig. 2 shows the AC-detector current as a function of spectrometer energy ΔE and magnetic field for an injection energy of $\delta E \approx 200\,\mu$eV. We first consider the magnetic field dependence. In Fig. 2a we observe a strong signal around $B = +18.5\,$mT. The corresponding radius of $3.6\,\mu$m matches the direct path between the dots as shown in the inset. We observe an additional maximum at 6 mT which is thought to be related to ballistic electrons undergoing a single scattering event with an impurity in the region between the quantum dots. The sub-structure of the ballistic peak itself possibly reflects the angular distribution of the injection.[13] We do not observe any strong signal at larger positive or at any negative magnetic fields. As an additional test of the ballistic nature of our signal we swapped the roles of source and detector dots. The result is shown in Fig. 2b and reveals a signal distribution which is nearly a mirror image of Fig. 2a with respect to $B = 0$. The main signal of direct ballistic electrons has swapped to $B = -18.5\,$mT as the ballistic path now has opposite curvature. Thus the magnetic field dependence proves convincingly the direct ballistic nature of the signals around $\pm 18\,$mT.

We now turn to the energy dependence. We inject ballistic electrons with an excess energy of $\delta E \approx 200\,\mu$eV, and indeed we observe in Fig. 2a a peak at $\Delta E \approx 200\,\mu$eV. Thus our spectrometer detects ballistic electrons at the correct energy. Additionally Fig. 2a reveals a large maximum at a lower energy $\delta E \approx 100\,\mu$eV. This might seem surprising at first glance as we expect to inject electrons only at one energy; but we can understand this by taking into account tunnelling through excited states of the detector dot which occurs at lower values of ΔE as depicted in Fig. 3a. Each excited state contributes to the measured spectrum a replica of the energy distribution of the impinging electrons at apparently lower energy . Hence we measure a convolution of the true signal with the response function of the detector, which we can model as a sum of weighted δ-functions. The different excitation spectra of QD1 and QD2 are responsible for the differences in the energy dependence of the measured currents in Fig. 2a and 2b.

The excitation energies of the dot and the respective tunnelling rates can be determined from transport spectroscopy of the detector quantum dot. The measurement

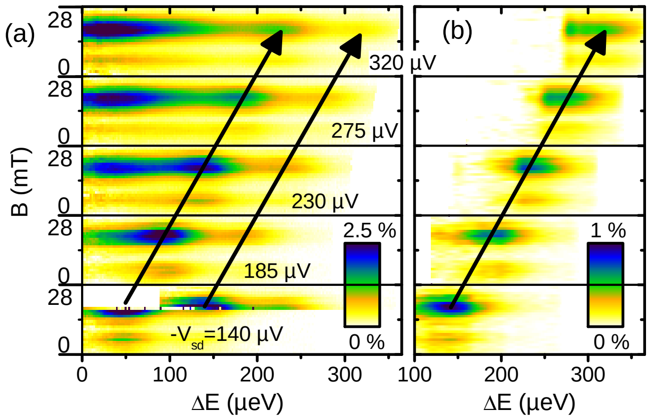

FIG. 4: a) Normalized detector signal for five different injector bias voltages. b) Result of the deconvolution taking into account two excited states. The arrows indicate the expected energy shift of the ballistic signal.

shown in Fig. 3b shows not only the ground state resonance with the source chemical potential (marked by a white line) but also resonances due to a strong excited state with excitation energy $\varepsilon_1 = 90\,\mu$eV (solid red line) and a further weak excited state at $\varepsilon_2 = 160\,\mu$eV (dotted red line, revealed by a negative $dI/dV_{\rm sd}$). We can estimate the ratio of the tunnelling rates as $r_1 = \Gamma_1/\Gamma_0 \approx 2.5$ and $r_2 = \Gamma_2/\Gamma_0 \approx 1$. We can now use these results to perform a deconvolution of the measured spectrum as follows: the desired signal which would be measured in the absence of excited states is represented by a equi-spaced cubic spline. The convolution of this trial function with the response function $\delta(E) + r_1\delta(E-\varepsilon_1) + r_2\delta(E-\varepsilon_2)$ is calculated, and a linear least-squares fit to the measured current then determines the spline coefficients and thus the spectrum. Fig. 3c shows the normalized detector current for a measurement with injection at $-eV_{\rm sd} = 230\,\mu$eV. The result of the deconvolution is displayed in Fig. 3d. The replica signals at lower energy were largely removed and the true spectrum of ballistic electrons with a narrow energy distribution is revealed.

Now we have demonstrated ballistic electron spectroscopy for a single injection energy, we proceed by varying the excess energy. Fig. 4 shows the spectra resulting from varying $\delta E = -eV_{\rm sd}$. For each $V_{\rm sd}$ value of the injector dot, its plunger gate voltage $V_{\rm p}$ was adjusted to achieve resonance of the injector level with the source chemical potential (Fig. 1). It is clear that the raw measured signal in Fig. 4a demonstrates the expected shift of the spectrum with increasing injection energy. This becomes even clearer in the deconvolved signal of Fig. 4b. Here we used the same tunnelling rate ratios $r_{1,2}$ as in Fig. 3d. Our simplified assumption of constant tunnelling rates accounts for the reduced quality of the deconvolution at high energies; a closer look to Fig. 3b reveals a voltage dependence of the conductance along the marked lines and thus a change of tunnelling rates. A more elaborate characterization of the detector dot would allow an improved quality of deconvolution.

Fig. 4 also reveals that the amplitude of the spectrometer signal at $\Delta E = \delta E = -eV_{\rm sd}$ falls with rising energy while the low energy signal near $\Delta E = 0$ increases. At the highest bias the reduction amounts to about 50 %. If we assume scattering as the only cause of signal reduction we deduce a scattering length of $l_s \sim 4\,\mu$m and a scattering time of about $\tau \sim 25$ ps. The predicted value for pure electron-electron scattering for excess energy $\delta E = 320\,\mu$eV and Fermi energy $E_F = 6$ meV is $l_{e-e} \sim 10\,\mu$m.[8,12] Further experiments are needed to test whether the smaller experimental value is caused by additional scattering or some other effect.

In conclusion, we have demonstrated the use of a quantum dot as a ballistic electron spectrometer. We have tested the scheme using a second quantum dot to source non-equilibrium ballistic electrons with a narrow energy and angle distribution. Using deconvolution techniques we can extract the spectrum even in the presence of excited states of the detector dot. The performance will increase further if we engineer the detector dot for larger excitation energy of a few 100 μeV.

Among the many potential applications of ballistic electron spectroscopy we can mention only a few: For quantum wires the position and movement of the subband energies could be measured near the 0.7 anomaly; the enhanced density of states of a quantum dot in the Kondo regime could be traced; resonant tunnelling involving non-equilibrium dot states could be characterized and the energy relaxation of non-equilibrium electrons could be measured in detail.

The authors would like to thank Abi Graham, Chris Ford and David Anderson. We acknowledge financial support from EPSRC and the European Union within the research training network COLLECT.

---

[1] J. Elzerman *et al.*, Nature **430**, 431 (2004).
[2] J. Petta *et al.*, Science **309**, 2180 (2005).
[3] N. K. Patel *et al.*, Phys. Rev. B **44**, 13549 (1991).
[4] L. P. Kouwenhoven *et al.*, NATO ASI series E **345**, 105 (1997).
[5] M. Heiblum, M. I. Nathan, D. C. Thomas, and C. M. Knoedler, Phys. Rev. Lett. **55**, 2200 (1985).
[6] A. Palevski *et al.*, Phys. Rev. Lett. **62**, 1776 (1989).
[7] P. Matthews *et al.*, et al., Phys. Rev. B **42**, 11415 (1990).
[8] A. Yacoby, U. Sivan, C. P. Umbach, and J. M. Hong, Phys. Rev. Lett. **66**, 1938 (1991).
[9] J. G. Williamson *et al.*, Phys. Rev. B **41**, 1207 (1990).
[10] A. S. Dzurak *et al.*, Phys. Rev. B **45**, 6309 (1992).
[11] T. J. Thornton, M. Pepper, H. Ahmed, D. Andrews, and G. J. Davies, Phys. Rev. Lett. **56**, 1198 (1986).
[12] G. F. Giuliani and J. J. Quinn, Phys. Rev. B **26**, 4421 (1982).
[13] Y. Oowaki *et al.*, Phys. Rev. B **47**, 4088 (1993).